VPS4A Mutations in Humans Cause Syndromic Congenital Dyserythropoietic Anemia due to Cytokinesis and Trafficking Defects

Katie G. Seu,[1,*] Lisa R. Trump,[2] Sana Emberesh,[2] Robert B. Lorsbach,[3,4] Clarissa Johnson,[5] Jessica Meznarich,[6,7] Hunter R. Underhill,[8,9] Stella T. Chou,[10,11] Haripriya Sakthivel,[1] Nicolas N. Nassar,[2,4] Kalani J. Seu,[12] Lionel Blanc,[13,14,15] Wenying Zhang,[4,16] Carolyn M. Lutzko,[2,4,17] and Theodosia A. Kalfa[1,4,*]

Summary

The Congenital Dyserythropoietic Anemia (CDA) Registry was established with the goal to facilitate investigations of natural history, biology, and molecular pathogenetic mechanisms of CDA. Three unrelated individuals enrolled in the registry had a syndrome characterized by CDA and severe neurodevelopmental delay. They were found to have missense mutations in *VPS4A,* a gene coding for an ATPase that regulates the ESCRT-III machinery in a variety of cellular processes including cell division, endosomal vesicle trafficking, and viral budding. Bone marrow studies showed binucleated erythroblasts and erythroblasts with cytoplasmic bridges indicating abnormal cytokinesis and abscission. Circulating red blood cells were found to retain transferrin receptor (CD71) in their membrane, demonstrating that VPS4A is critical for normal reticulocyte maturation. Using proband-derived induced pluripotent stem cells (iPSCs), we have successfully modeled the hematologic aspects of this syndrome *in vitro*, recapitulating their dyserythropoietic phenotype. Our findings demonstrate that *VPS4A* mutations cause cytokinesis and trafficking defects leading to a human disease with detrimental effects to erythropoiesis and neurodevelopment.

The congenital dyserythropoietic anemias (CDAs) are a heterogeneous group of rare genetic disorders of erythropoiesis with distinct morphologic abnormalities of late erythroblasts in the bone marrow, including bi- and multinucleated cells.[1,2] Individuals present with a variable degree of anemia with clinical and laboratory findings of hemolysis, indicating not only impaired production but also decreased survival of the abnormally produced red blood cells (RBCs). Associated iron overload disproportionate to the number of transfusions is a hallmark of ineffective erythropoiesis. To date, there are six genes known to be associated with CDA: *CDAN1* (MIM: 607465), *CDIN1* ([MIM: 615626], previously known as *C15ORF41*), *SEC23B* (MIM: 610512), *KIF23* (MIM: 605064), *KLF1* (MIM: 600599), and *GATA1* (MIM: 305371);[2,3] however, many individuals with CDA remain without an identified genetic diagnosis (non-typable CDA). Through the CDA registry for North America (CDAR; ClinicalTrials.gov/NCT02964494), we identified three unrelated probands with a syndrome characterized by congenital dyserythropoietic anemia and neurodevelopmental disorder who were found to have different missense mutations in *VPS4A* (MIM: 609982).

Vacuolar Protein Sorting 4A (VPS4A) is one of two human homologs of the yeast protein Vps4 and member of the AAA protein family (ATPases associated with diverse cellular activities). It is recruited by the endosomal sorting complexes required for Transport (ESCRT)-III machinery to sites of membrane remodeling and vesicle formation.[4] *VPS4* was first identified in yeast to be required for endosomal vesicle transport and receptor recycling[5] and has since been shown to participate in a variety of cellular processes including viral budding,[6] exosome biogenesis,[7] and cell division.[8] VPS4A and its paralog VPS4B have been shown to concentrate at the spindle poles during metaphase and at the midbody during the abscission stage of cytokinesis in HeLa cells; knockdown of either resulted in defects in abscission, centrosome number, and nuclear

[1]Division of Hematology, Cancer and Blood Diseases Institute, Cincinnati Children's Hospital Medical Center, Cincinnati, OH 45229, USA; [2]Division of Experimental Hematology and Cancer Biology, Cancer and Blood Diseases Institute, Cincinnati Children's Hospital Medical Center, Cincinnati, OH 45229, USA; [3]Division of Pathology, Cincinnati Children's Hospital Medical Center, Cincinnati, OH 45229, USA; [4]Department of Pediatrics, University of Cincinnati College of Medicine, Cincinnati, OH 45229, USA; [5]Pediatric Hematology-Oncology Cook Children's Medical Center, Fort Worth, TX 76104, USA; [6]Division of Hematology-Oncology, Department of Pediatrics, University of Utah, Salt Lake City, UT 84132, USA; [7]Primary Children's Hospital, Intermountain Healthcare, Salt Lake City, UT 84113, USA; [8]Division of Medical Genetics, Department of Pediatrics, University of Utah, Salt Lake City, UT 84108, USA; [9]Department of Radiology, University of Utah, Salt Lake City, UT 84108, USA; [10]Division of Hematology, Children's Hospital of Philadelphia, Philadelphia, PA 19104, USA; [11]Department of Pediatrics, Perelman School of Medicine, University of Pennsylvania, Philadelphia, PA 19104, USA; [12]Department of Chemistry, Earlham College, Richmond, IN 47374, USA; [13]Laboratory of Developmental Erythropoiesis, Center for Autoimmune, Musculoskeletal and Hematopoietic Diseases, Institute of Molecular Medicine, The Feinstein Institutes for Medical Research, Manhasset, NY 11030, USA; [14]Les Nelkin Memorial Pediatric Oncology Laboratory, Institute of Molecular Medicine, The Feinstein Institutes for Medical Research, Manhasset, NY 11030, USA; [15]Department of Molecular Medicine and Pediatrics, Zucker School of Medicine at Hofstra/Northwell, Hempstead, NY 11549, USA; [16]Laboratory of Genetics and Genomics, Division of Human Genetics, Cincinnati Children's Hospital Medical Center, Cincinnati, OH 45229, USA; [17]Hoxworth Blood Center, University of Cincinnati College of Medicine, Cincinnati, OH 45229, USA
*Correspondence: katie.giger@cchmc.org (K.G.S.), theodosia.kalfa@cchmc.org (T.A.K.)
https://doi.org/10.1016/j.ajhg.2020.10.013.

Table 1. Clinical and Laboratory Findings in the CDAR-Enrolled Probands with *VPS4A* Mutations

	VPS4A (NM_013245.2) Mutations	Age, Sex, & Ethnic Background	Laboratory Findings			Ferritin (F) / LIC	Age at First Transfusion	Transfusion Requirement	Non-hematologic findings
			Lowest Hb	ARC	MCV				
1	*de novo* c.850A>T (p.Arg284Trp) heterozygous	6 y.o., F, European- and Hispanic-American	7.3 (increased irritability when anemia worsens)	380–500	89–98	F 840, LIC 12.1 at 4y.o., now controlled with deferasirox	neonate (EGA 35 wks)	every 4–6 weeks	severe global developmental delay, microcephaly, microgyria, dystonia (axial hypotonia with appendicular hypertonia), suspected Leber congenital amaurosis and/or cortical blindness, failure to thrive, frequent urinary tract infections
2	*de novo* c.608G>A (p.Gly203Glu) heterozygous	5 y.o., M, European- and Hispanic-American	6.1	40–500	80–100	F 4093, LIC 8.82 at 5y.o., on deferasirox	neonate (EGA 34 wks)	every 4–10 weeks	severe global developmental delay, seizure disorder, microcephaly, microgyria, dystonia (axial hypotonia with appendicular hypertonia), congenital bilateral cataracts, failure to thrive, chronic kidney disease (stage II-III)
3	c.83C>T (p.Ala28Val) homozygous	3 y.o., F, Arabic	6.9	240–400	88–99	F 470 LIC 6.5, at 2.5 y.o. before starting deferasirox	neonate (EGA 35 wks) exchange transfusion for hyperbilirubinemia	occasionally (every 2–6 months)	global developmental delay, macrocephaly, dystonia (axial hypotonia with appendicular hypertonia), delayed myelination, esotropia, frequent urinary tract infections

Abbreviations, normal range, and units: y.o., years old; Hb, hemoglobin concentration (11.5–13.5 g/dL); ARC, absolute reticulocyte count (29–80 $10^6/\mu L$); MCV, mean corpuscular volume (75–87 fL); F, serum ferritin (10–150 ng/mL); LIC, liver iron content (<2.4 mg/g dry liver weight) based on T2* MRI or Ferriscan; EGA, estimated gestation age. All the probands were noted at birth to have hepatomegaly and cholestasis that gradually improved. They have persistent splenomegaly.

morphology, making VPS4A an attractive candidate cause of CDA.[9]

Three individuals enrolled in CDAR, after written informed consent was provided by the families (details included in the Supplemental Material and Methods), were noted to have non-typable CDA with a similar syndromic phenotype (Table 1). In addition to CDA pathology in bone marrow studies and laboratory findings indicating macrocytic hemolytic anemia with brisk reticulocytosis, splenomegaly, and accelerated iron overload disproportionate to the volume of RBC transfusions received, all three children had a significant neurodevelopmental disorder, similar to the one described in detail by Rodger et al.[10] The first two probands had severe global developmental delay and congenital microcephaly with brain MRI showing moderate to marked deficiency of hemispheric white matter with global cerebral volume loss, thin corpus callosum, and atrophy of the cerebellum and the pons, suggestive of a neurodegenerative syndrome (Figure S1). The third proband, offspring of consanguineous parents, had a milder hematologic phenotype, requiring after infancy fewer than four transfusions yearly, typically due to hemolytic crises usually with a febrile illness. She had a static developmental age of 6–8 months with brain MRI showing also diffuse prominence of all supratentorial ventricles and subarachnoid fluid spaces *ex vacuo*, thin corpus callosum, diffuse cerebral gray and white matter parenchymal volume loss, and delay in white matter myelination (Figure S1).

Probands 1 and 2 had transfusion-dependent anemia with bone marrow studies showing 3%–7% binucleated erythroblasts (Figure 1A), initially thought to have CDA-I (MIM: 224120). Interestingly, cytoplasmic bridges were observed, rather than the nuclear bridges typically seen in CDA-I.[11] Proband 3 had fewer binucleated erythroblasts in her bone marrow aspirate (Figure 1A), compatible with her milder hematologic phenotype. Nevertheless, she had accelerated iron overload indicative of ineffective erythropoiesis.

Next generation sequencing (NGS) and deletion/duplication analysis by comparative genomic hybridization on a panel of genes for hereditary hemolytic anemias due to RBC membrane disorders, enzymopathies, and CDAs did not reveal a causative mutation; therefore, whole-exome

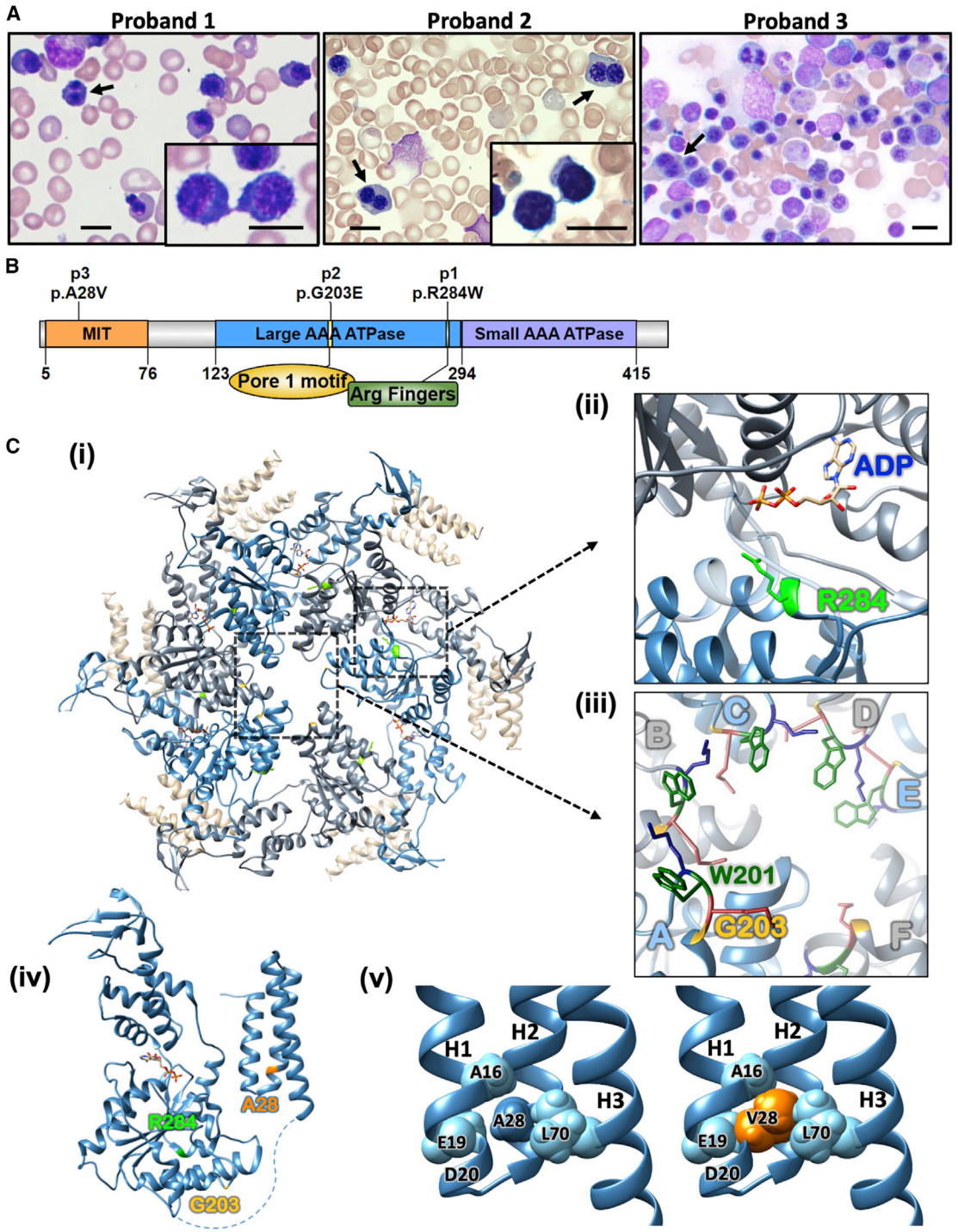

Figure 1. Genotype and Erythroid Phenotype of Individuals with *VPS4A* Mutations

(A) Bone marrow aspirate smears from each proband showing erythroid hyperplasia. Erythroblasts show megaloblastoid changes and include cells with binucleation (arrows) and cytoplasmic bridges joining erythroblasts post-division, noted especially in probands 1 and 2 (insets). Scale bar 10 μm.

(B) Diagram of VPS4A protein structure. The N-terminal MIT domain is followed by a flexible linker and an ATPase cassette consisting of a large and small ATPase domain and a β-domain. The location of the mutations found in the probands is marked.

(C) (i) Ribbon diagram of Vps4 proteins assembled in a hexamer (PDB: 6AP1). Residues mutated in the probands are colored green (Arg284 [R284] in p1) and yellow (Gly203 [G203] in p2). The numbering for human VPS4A is used, depicting the homologous residues in the yeast Vps4. Insets show (ii) the ADP in binding site at the interface of two adjacent subunits (blue and gray) with Arg284 (R284 in green) and (iii) the central pore of the hexamer where Gly203 (G203 in yellow) in the pore loop is crucial for the arrangement of Trp201 (W201 in dark green) forming hydrophobic binding pockets for ESCRT-III proteins passing through the central pore.[12] (iv) Ribbon diagram of a Vps4 monomer based on PDB: 6AP1 for yeast Vps4 and PDB: 1YXR for human MIT domain. Residues mutated in the

(legend continued on next page)

sequencing (WES) was performed for each proband in a family-trio design. Probands 1 and 2 were each found to have a single *de novo* heterozygous missense mutation in *VPS4A* (GenBank: NM_013245.2): c.850A>T (p.Arg284Trp) and c.608G>A (p.Gly203Glu), respectively, affecting residues in the highly conserved large ATPase domain of VPS4A. Proband 3 had the homozygous *VPS4A* (GenBank: NM_013245.2) mutation c.83C>T (p.Ala28Val), occurring in the N-terminal microtubule interacting and trafficking domain (MIT) (Table 1 and Figures 1B and 1C). Her asymptomatic parents were heterozygous for this variant and had a normal hematologic phenotype. The *VPS4A* variants found in the probands have not been reported in HGMD, ClinVar, or NCBI variant databases and were absent in the ExAC and gnomAD v2.1.1 and v3 control population databases. All affected amino acid residues are highly conserved across species down to yeast (Figure S2) and the *in silico* prediction for the substitutions were probably damaging (PolyPhen-2), deleterious (SIFT), and disease causing (MutationTaster).

Via its MIT domain, Vps4 binds to ESCRT-III subunits through their MIT interacting motif (MIM). This promotes the assembly of Vps4 into a ring-shaped hexamer (Figure 1Ci), resulting in the generation of an active enzyme. The ESCRT-III filaments then bind within the pore at the center of the hexamer and ATP hydrolysis drives their translocation through the pore, constricting and ultimately disassembling ESCRT-III in order to achieve membrane fission.[14–17] Since VPS4A is 60% similar to Vps4 and shares its highly conserved functional domains, we have used this model, built upon cryo-EM studies,[16] to visualize the location and potential impact of the mutations found in the probands discussed here.

VPS4A c.850A>T (p.Arg284Trp) is a mutation of the penultimate base of exon 8 and multiple splice prediction algorithms suggested it may affect the splice donor site of intron 8. However, PCR-amplification performed on cDNA generated from proband 1-reticulocyte mRNA followed by Sanger sequencing of the single band in the gel confirmed that this is a missense and not a splicing variant (Figure S3). The Arg284 residue is one of two arginine fingers functioning in the ATP binding pocket.[14] The arginine fingers from one subunit protrude into the ATP binding pocket of the adjacent subunit (Figure 1Cii) and interact with the γ-phosphate of ATP, promoting hydrolysis.[18] Therefore, alteration of Arg284 would be expected to compromise ATP hydrolysis and the function of VPS4A as an ATPase. The Gly203 residue altered in proband 2 is part of the pore loop 1 motif which forms the central pore of the active hexamer. The glycine at this position is highly conserved, as it is the only amino acid that permits the packing and conformation required for the adjacent pore loop 1 residues Trp201 and Leu202 to create binding pockets for the sidechains of the ESCRT-III subunits passing through the pore (Figure 1Ciii).[4,12] Site-directed mutagenesis of Gly203 to even an alanine (p.Gly203Ala) in human VPS4A has been shown to cause loss of function, inhibiting viral budding *in vitro*.[19] The Ala28 residue in the N-terminal MIT domain of VPS4A, altered by both alleles in proband 3, is one of a series of conserved alanines that form an "alanine zipper," which bundles together the 3 helices of the MIT domain (Figure 1Civ).[20] Binding of this domain to the MIMs of ESCRT-III proteins is considered necessary for hexamer formation and enzyme activation.[4] Modeling of Val at position 28 in the structure of the MIT domain of human VPS4A results in steric clashes with several amino acid side chains in both helices 1 (H1) and 3 (H3), as well as the backbone of H1 (Figure 1Cv). Thus, the p.Ala28Val variant may affect VPS4A function by altering MIT domain structure. Further studies will be necessary to demonstrate whether this affects interaction with MIM1 or MIM2 domains, or both, and what impact this has on assembly and activity of the ESCRT-III complex.[15,21]

Based on the pedigree and the clinical findings in proband 3, this variant appears pathogenic only when homozygous. Although still within the spectrum of the same syndrome, the phenotype is somewhat milder than the clinical picture secondary to *de novo* heterozygous variants in the large ATPase domain which appear to exert a more detrimental, dominant-negative effect,[10,22] demonstrating evidence of genotype-phenotype correlation. The homozygous p.Ala28Val variant in proband 3 putatively disrupts VPS4A interaction with ESCRT-III proteins due to altered structure of the MIT domain, rather than directly affecting its ATPase activity.

To investigate the impact of the identified variants on VPS4A function in erythroid cells, we evaluated the transferrin receptor (CD71) downregulation on the reticulocyte membrane in the probands' blood samples, a process dependent on normal endosomal sorting and exosome secretion.[23,24] We examined the peripheral RBCs by flow cytometry for cell surface expression of CD71 utilizing thiazole orange (TO) to label the RNA-containing reticulocytes. All three probands had a unique population of $CD71^{+}/TO^{-}$ cells not typically observed in control samples (Figure 2A). Using imaging flow cytometry (IFC), we could see that this population included mature biconcave RBCs (Figure S4) which do not normally carry CD71 on their membrane. A relative decrease in the proportion of more mature $CD71^{-}/TO^{+}$ reticulocytes was also noted (Figure 2B). Together, these data demonstrate defective CD71 trafficking associated with either of the VPS4A

probands are colored green (Arg284 [R284] in p1), yellow (Gly203 [G203] in p2), and orange (Ala28 [A28] in p3). (v) The structure of human VPS4A MIT domain (PDB: 1YXR) with Ala28 (A28) and neighboring residues shown as spheres (left). Modeling of the Val28 variant (orange) found in p3 demonstrates clashes with the side chains of Leu70 and Glu19, as well as the main chain of Ala16 and Asp20 (side chain not shown for clarity) (right). All protein structure figures were generated with UCSF Chimera.[13]

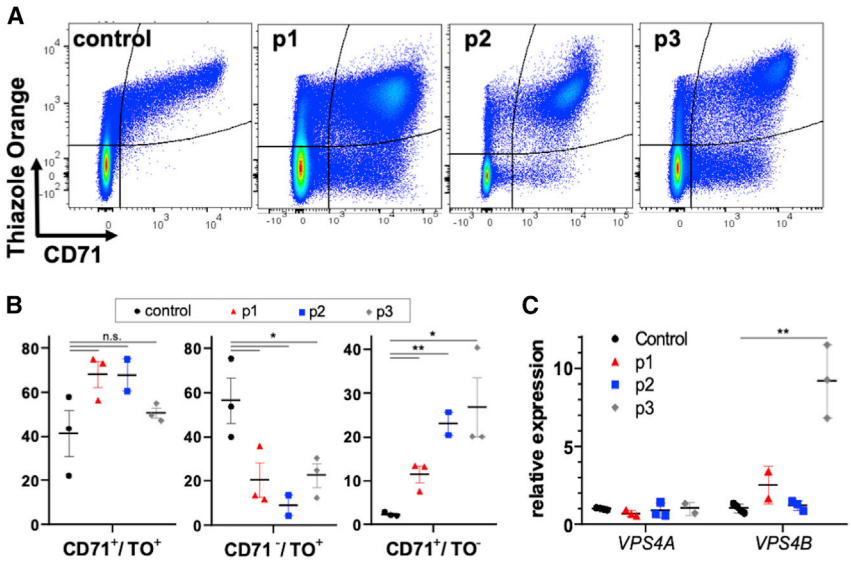

Figure 2. Peripheral Blood Phenotype of Probands with *VPS4A* Mutations

(A) Flow cytometry analysis of probands' peripheral RBCs ($CD45^-$) showing presence of an unusual population positive for transferrin receptor ($CD71^+$) and negative for RNA, as labeled by thiazole orange (TO).

(B) Quantification of immature RBC populations analyzed by flow cytometry and IFC ($CD71^+/TO^+$, $CD71^-/TO^+$, and $CD71^+/TO^-$) as a percentage of total $CD71^+$ and/or TO^+ cells (excluding all mature $CD71^-/TO^-$ RBCs since probands 1 and 2 are regularly transfused). Samples from individuals with sickle cell disease (SCD) were used as positive controls with increased reticulocyte counts. Data shown are mean ± SEM of n = 3 experiments for all but p2 (n = 2). * $p < 0.05$ and ** $p < 0.01$ by a Student's t test for samples with unequal variance.

(C) Relative expression of *VPS4A* and *VPS4B* in $CD71^+$ reticulocytes isolated from whole blood and evaluated by qPCR. Data are mean ± SEM, n = 4 control; n = 3 p1&2 VPS4A, p2&3 VPS4B; n = 2 p1 *VPS4B*, p3 *VPS4A*, ** $p < 0.01$ by a Student's t test for samples with unequal variance.

heterozygous variants p.Arg284Trp or p.Gly203Glu or the homozygous p.Ala28Val variant, consistent with the observation of abnormal endosomal compartments in VPS4A p.Arg284Trp mutant fibroblasts by Rodger et al.[10]

The levels of expression for *VPS4A* and *VPS4B* (MIM: 609983) vary between different mammalian tissues; in mice, most tissues show a strong bias for one of the two Vps4 proteins.[25] This tissue specificity may explain the predominance of neurological and erythroid lineage manifestations in the syndrome described. Since the two human VPS4 paralogs share 80% similarity in their sequence, they may be able to compensate for each other through redundancy of function or even interaction and assembly into mixed hexamers.[22] Therefore, we evaluated by quantitative PCR the expression of *VPS4A* and *VPS4B* in $CD71^+$ reticulocytes isolated from the probands' peripheral blood. While *VPS4A* expression was not significantly affected by any of the mutations, we observed significantly increased *VPS4B* expression in proband 3 (Figure 2C), indicating that VPS4B may partially, but not adequately, compensate for the VPS4A loss of function in the homozygous p.Ala28Val variant, possibly contributing to the milder disease phenotype.

In order to model the probands' bone marrow disease *in vitro*, we optimized a culture protocol to differentiate iPSCs, generated from peripheral blood mononuclear cells (PBMNCs), to hematopoietic progenitors and then to erythroblasts, and compared the erythroblasts produced from proband 1-derived iPSCs, carrying heterozygous VPS4A p.Arg284Trp, with erythroblasts produced from healthy control donor iPSCs (Figure 3). iPSCs derived from an individual with CDA-I due to compound heterozygous *CDAN1* mutations[26] were used in two of the experiments as a positive (diseased) control. The culture schema and the hematopoietic and erythroid differentiation are shown in Figures 3A–3C, while statistics for each population demonstrating the repeatability of the process are detailed in Tables S1 and S2. iPSCs were differentiated for the first 10 days of the culture into hematopoietic progenitor cells identified as $CD43^+/CD41^+/GPA^+$ (Figure 3B), which were then harvested and placed into serum-free medium containing stem cell factor (SCF), erythropoietin (Epo), and dexamethasone for *ex vivo* erythropoiesis. After 5 days (day 10+5), the cells had lost CD41 and CD34 but retained GPA as they had differentiated into proerythroblasts based on flow cytometry analysis that monitors erythroid differentiation using GPA, Band 3, and α_4 integrin (Figures 3B and 3C).[27] On day 10+5, normal control cells were typically 40%–60% GPA^+ and out of those, 60%–75% were proerythroblasts (α_4^{high}/Band 3^-). At this point, SCF was removed and the Epo-containing medium was supplemented with human serum, supporting further erythroblast differentiation. After 3 days (day 10+8), the cells were >65% GPA^+ and primarily $\alpha_4^{high/mid}$/Band 3^+ consistent with late basophilic to polychromatophilic erythroblasts (Figure 3C), at which point cells were fixed for morphology evaluation by IFC. *Ex vivo* erythropoiesis from iPSCs with VPS4A p.Arg284Trp heterozygous variant was less synchronous in comparison to control and the erythroblasts matured more rapidly than controls (Figure 3D). Cytospins indicated increased frequency of binucleated erythroblasts (Figure 3E) while poor growth was evident in the proband-derived culture, similar to the CDAN1 mutant cells and in contrast to a brisk growth in the normal control culture (Figure 3F).

To evaluate the role of VPS4 proteins in erythroblast division, we first examined the localization of VPS4A/B in dividing erythroblasts cultured from normal human

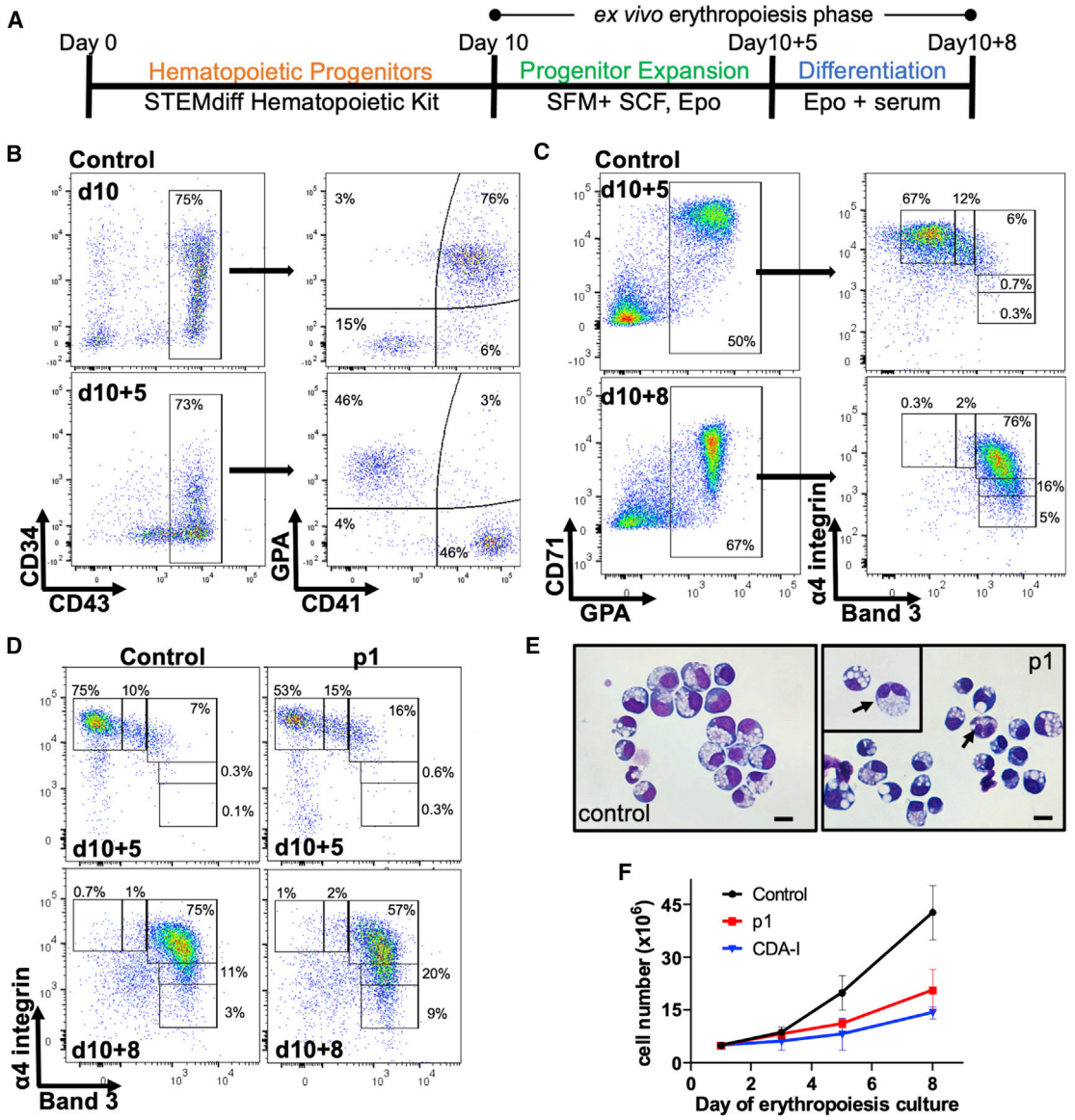

Figure 3. Proband-Derived iPSCs Recapitulate the Clinical Phenotype of Dyserythropoiesis
(A) Schematic of iPSC differentiation into hematopoietic progenitors followed by *ex vivo* erythropoiesis.
(B) Flow cytometry analysis of the $CD43^+/CD41^+/GPA^+$ hematopoietic progenitors harvested on day 10 from control iPSCs.
(C) Flow cytometry analysis of control iPSC-derived erythroblasts by GPA, α_4 integrin, and Band 3.
(D) Flow cytometry analysis of erythroblasts produced in *ex vivo* erythropoiesis cultures from control- and p1-derived iPSCs.
(E) Wright-stained cytospins from day 10+8 cultures (arrows indicate binucleated erythroblasts). Scale bar 10 μm.
(F) Average growth curves for iPSC lines used in the *ex vivo* erythropoiesis phase of the culture (mean ± SEM, n = 4 for control and p1; n = 2 for cultures initiated from CDA-I iPSCs).

$CD34^+$ cells using an antibody that recognizes both VPS4A and VPS4B. By IFC, we found that VPS4 localized to the spindle poles and midbody of dividing erythroblasts (Figure 4A), as has been previously described in HeLa cells.[9] VPS4 was also detected in the midbody during abscission in erythroblasts produced from both control and proband iPSC cultures (Figure 4B, panels 1–3); however, in control cells, VPS4 was present throughout the midbody, while in the proband line, VPS4 typically did not extend into the midbody with tubulin evident through gaps in VPS4 staining (Figures 4B and 4C). In addition, persistent cytoplasmic bridges between erythroblasts were often observed in proband 1 cultures even after attempted completion of cytokinesis, as assessed by the lack of a tubulin-based midbody structure (Figure 4B, panel 4). These erythroid cells appear very similar to those present in the proband's bone marrow aspirate (Figure 1A insets) and were confirmed by confocal microscopy to be devoid of DNA (Figure 4D). Erythroblasts cultured from proband 1-derived iPSCs were verified by IFC to have a higher incidence of binucleation (Figures 4E and 4F).

In summary, we have identified *VPS4A* as a gene associated with congenital dyserythropoietic anemia in three unrelated probands with a syndrome characterized

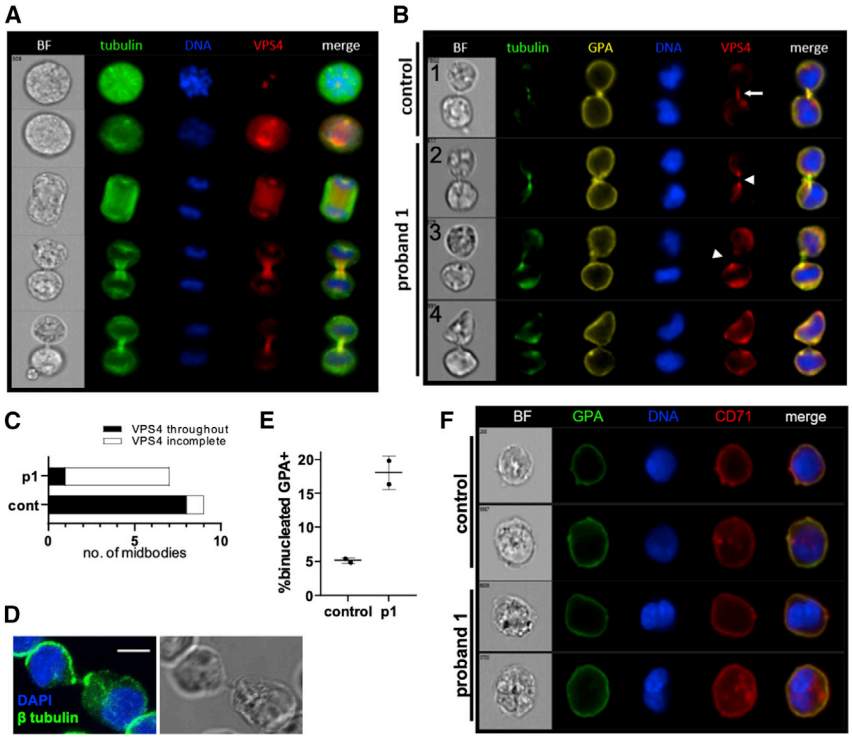

Figure 4. VPS4A Is Critical for Normal Erythroblast Cytokinesis

(A) Imaging flow cytometry (IFC) analysis of VPS4 localization in dividing erythroblasts cultured from normal human CD34$^+$ cells showing β-tubulin (green), DNA/Hoechst (blue), and VPS4 (red).

(B) Representative images of erythroblasts produced from control and proband 1-derived iPSCs undergoing cytokinesis showing congruent staining of VPS4 (red) and tubulin (green) in the midbody of control cells (panel 1) but mislocalization of VPS4 relative to tubulin in p1-derived erythroblasts (panels 2 and 3). Post-mitotic erythroblasts with mutant *VPS4A* are frequently observed to remain connected with persistent cytoplasmic bridges, indicating abscission failure (panel 4).

(C) Analysis of VPS4 localization in midbodies demonstrated that VPS4 was present throughout the midbody in 8 out of 9 events observed in control cells, but only in 1 out of 7 events observed in the proband line.

(D) Confocal immunofluorescence imaging of an erythroblast generated *in vitro* from proband 1-derived iPSCs with a cytoplasmic bridge containing no DNA (blue). Scale bar 5 μm.

(E) A higher frequency of binucleated erythroblasts was observed in proband 1-derived iPSC cultures versus control (>300 cells analyzed by IFC out of two biologic repeats, mean ± SEM).

(F) Representative IFC images of normal nuclei in control erythroblasts and binucleated erythroblasts from *ex vivo* erythropoiesis cultures from control and proband 1-derived iPSCs.

by CDA and severe neurodevelopmental delay. Using proband-derived iPSCs we have modeled the hematologic aspects of the disease *in vitro*, recapitulating the dyserythropoietic phenotype, and developed an *in vitro* system to facilitate further studies in CDA and other diseases of terminal erythropoiesis. Our findings demonstrate that normal function of VPS4A is essential for human erythropoiesis.

Data and Code Availability

The variants identified in this work have been submitted to ClinVar (submission ID: SUB8385045). WES datasets have not been deposited in a public repository due to privacy and ethical restrictions.

Supplemental Data

Supplemental Data can be found online at https://doi.org/10.1016/j.ajhg.2020.10.013.

Acknowledgments

We thank the families for their generous participation in CDAR. We thank Drs. Jose Cancelas, Mohandas Narla, and Yi Zheng for their valuable advice. Molecular graphics and analyses performed with UCSF Chimera, developed by the Resource for Biocomputing, Visualization, and Informatics at the University of California, San Francisco, with support from NIH P41-GM103311.[13] All flow cytometric data were acquired using equipment maintained by the Research Flow Cytometry Core in the Division of Rheumatology at Cincinnati Children's Hospital Medical Center. Healthy donor cells were provided by the Cell Processing Core in Division of Experimental Hematology and Cancer Biology. This work was supported by the National Institutes of Health, National Heart, Lung, and Blood Institute grant R01HL116352 (T.A.K.), National Institute of General Medical Sciences grant R01GM110628 (C.M.L.), the Cincinnati Children's Hospital CPG (Center for Pediatric Genomics), and CuSTOM (Center for Stem Cell & Organoid Medicine) funding awards.

Declaration of Interests

The authors declare no competing interests.

Received: July 3, 2020
Accepted: October 26, 2020
Published: November 12, 2020

Web Resources

CDAR clinical trial, https://clinicaltrials.gov/ct2/show/NCT02964494
European Molecular Biology Laboratory (EMBL-EBI), https://www.ebi.ac.uk/Tools/msa/clustalo/
Online Mendelian Inheritance in Man, https://www.omim.org
Protein Data Bank, https://www.rcsb.org/
UCSF Chimera Molecular Modeling, https://www.cgl.ucsf.edu/chimera/

References

1. Heimpel, H., and Wendt, F. (1968). Congenital dyserythropoietic anemia with karyorrhexis and multinuclearity of erythroblasts. Helv. Med. Acta *34*, 103–115.
2. Iolascon, A., Heimpel, H., Wahlin, A., and Tamary, H. (2013). Congenital dyserythropoietic anemias: molecular insights and diagnostic approach. Blood *122*, 2162–2166.
3. Risinger, M., Emberesh, M., and Kalfa, T.A. (2019). Rare Hereditary Hemolytic Anemias: Diagnostic Approach and Considerations in Management. Hematol. Oncol. Clin. North Am. *33*, 373–392.
4. McCullough, J., Frost, A., and Sundquist, W.I. (2018). Structures, Functions, and Dynamics of ESCRT-III/Vps4 Membrane Remodeling and Fission Complexes. Annu. Rev. Cell Dev. Biol. *34*, 85–109.
5. Babst, M., Sato, T.K., Banta, L.M., and Emr, S.D. (1997). Endosomal transport function in yeast requires a novel AAA-type ATPase, Vps4p. EMBO J. *16*, 1820–1831.
6. Baumgärtel, V., Ivanchenko, S., Dupont, A., Sergeev, M., Wiseman, P.W., Kräusslich, H.G., Bräuchle, C., Müller, B., and Lamb, D.C. (2011). Live-cell visualization of dynamics of HIV budding site interactions with an ESCRT component. Nat. Cell Biol. *13*, 469–474.
7. Hessvik, N.P., and Llorente, A. (2018). Current knowledge on exosome biogenesis and release. Cell. Mol. Life Sci. *75*, 193–208.
8. Mierzwa, B.E., Chiaruttini, N., Redondo-Morata, L., von Filseck, J.M., König, J., Larios, J., Poser, I., Müller-Reichert, T., Scheuring, S., Roux, A., and Gerlich, D.W. (2017). Dynamic subunit turnover in ESCRT-III assemblies is regulated by Vps4 to mediate membrane remodelling during cytokinesis. Nat. Cell Biol. *19*, 787–798.
9. Morita, E., Colf, L.A., Karren, M.A., Sandrin, V., Rodesch, C.K., and Sundquist, W.I. (2010). Human ESCRT-III and VPS4 proteins are required for centrosome and spindle maintenance. Proc. Natl. Acad. Sci. USA *107*, 12889–12894.
10. Rodger, C., Flex, E., Allison, R.J., Sanchis-Juan, A., Hasenahuer, M.A., Cecchetti, S., French, C.E., Edgar, J.R., Carpentieri, G., Ciolfi, A., et al. (2020). De novo VPS4A mutations cause multisystem disease with abnormal neurodevelopment. Am. J. Hum. Genet. *107*, this issue, 1129–1148.
11. Tamary, H., Dgany, O., Proust, A., Krasnov, T., Avidan, N., Eidelitz-Markus, T., Tchernia, G., Geneviève, D., Cormier-Daire, V., Bader-Meunier, B., et al. (2005). Clinical and molecular variability in congenital dyserythropoietic anaemia type I. Br. J. Haematol. *130*, 628–634.
12. Han, H., Monroe, N., Sundquist, W.I., Shen, P.S., and Hill, C.P. (2017). The AAA ATPase Vps4 binds ESCRT-III substrates through a repeating array of dipeptide-binding pockets. eLife *6*, 6.
13. Pettersen, E.F., Goddard, T.D., Huang, C.C., Couch, G.S., Greenblatt, D.M., Meng, E.C., and Ferrin, T.E. (2004). UCSF Chimera–a visualization system for exploratory research and analysis. J. Comput. Chem. *25*, 1605–1612.
14. Han, H., and Hill, C.P. (2019). Structure and mechanism of the ESCRT pathway AAA+ ATPase Vps4. Biochem. Soc. Trans. *47*, 37–45.
15. Adell, M.A.Y., Vogel, G.F., Pakdel, M., Müller, M., Lindner, H., Hess, M.W., and Teis, D. (2014). Coordinated binding of Vps4 to ESCRT-III drives membrane neck constriction during MVB vesicle formation. J. Cell Biol. *205*, 33–49.
16. Monroe, N., Han, H., Shen, P.S., Sundquist, W.I., and Hill, C.P. (2017). Structural basis of protein translocation by the Vps4-Vta1 AAA ATPase. eLife *6*, 6.
17. Su, M., Guo, E.Z., Ding, X., Li, Y., Tarrasch, J.T., Brooks, C.L., 3rd, Xu, Z., and Skiniotis, G. (2017). Mechanism of Vps4 hexamer function revealed by cryo-EM. Sci. Adv. *3*, e1700325.
18. Wendler, P., Ciniawsky, S., Kock, M., and Kube, S. (2012). Structure and function of the AAA+ nucleotide binding pocket. Biochim. Biophys. Acta *1823*, 2–14.
19. Scott, A., Chung, H.Y., Gonciarz-Swiatek, M., Hill, G.C., Whitby, F.G., Gaspar, J., Holton, J.M., Viswanathan, R., Ghaffarian, S., Hill, C.P., and Sundquist, W.I. (2005). Structural and mechanistic studies of VPS4 proteins. EMBO J. *24*, 3658–3669.
20. Scott, A., Gaspar, J., Stuchell-Brereton, M.D., Alam, S.L., Skalicky, J.J., and Sundquist, W.I. (2005). Structure and ESCRT-III protein interactions of the MIT domain of human VPS4A. Proc. Natl. Acad. Sci. USA *102*, 13813–13818.
21. Kieffer, C., Skalicky, J.J., Morita, E., De Domenico, I., Ward, D.M., Kaplan, J., and Sundquist, W.I. (2008). Two distinct modes of ESCRT-III recognition are required for VPS4 functions in lysosomal protein targeting and HIV-1 budding. Dev. Cell *15*, 62–73.
22. Scheuring, S., Röhricht, R.A., Schöning-Burkhardt, B., Beyer, A., Müller, S., Abts, H.F., and Köhrer, K. (2001). Mammalian cells express two VPS4 proteins both of which are involved in intracellular protein trafficking. J. Mol. Biol. *312*, 469–480.
23. Blanc, L., and Vidal, M. (2010). Reticulocyte membrane remodeling: contribution of the exosome pathway. Curr. Opin. Hematol. *17*, 177–183.
24. Géminard, C., De Gassart, A., Blanc, L., and Vidal, M. (2004). Degradation of AP2 during reticulocyte maturation enhances binding of hsc70 and Alix to a common site on TFR for sorting into exosomes. Traffic *5*, 181–193.
25. Beyer, A., Scheuring, S., Müller, S., Mincheva, A., Lichter, P., and Köhrer, K. (2003). Comparative sequence and expression analyses of four mammalian VPS4 genes. Gene *305*, 47–59.
26. Dgany, O., Avidan, N., Delaunay, J., Krasnov, T., Shalmon, L., Shalev, H., Eidelitz-Markus, T., Kapelushnik, J., Cattan, D., Pariente, A., et al. (2002). Congenital dyserythropoietic anemia type I is caused by mutations in codanin-1. Am. J. Hum. Genet. *71*, 1467–1474.
27. Hu, J., Liu, J., Xue, F., Halverson, G., Reid, M., Guo, A., Chen, L., Raza, A., Galili, N., Jaffray, J., et al. (2013). Isolation and functional characterization of human erythroblasts at distinct stages: implications for understanding of normal and disordered erythropoiesis in vivo. Blood *121*, 3246–3253.